

Rotational Stiffness Study of Two-Element Tethered Coulomb Structures

Carl R. Seubert and Hanspeter Schaub

University of Colorado, Boulder, CO, 80309

Simulated Reprint from

Journal of Spacecraft and Rockets

Volume 48, Number 3, May–June, 2011, Pages 488–497



A publication of the
American Institute of Aeronautics and Astronautics, Inc.
1801 Alexander Bell Drive, Suite 500
Reston, VA 22091

Rotational Stiffness Study of Two-Element Tethered Coulomb Structures

Carl R. Seubert* and Hanspeter Schaub †

University of Colorado, Boulder, CO, 80309

Combining features of large space structures and free-flying formations has led to the tethered Coulomb structure concept. Utilizing Coulomb forces to repel a formation of spacecraft nodes that are connected with fine tethers can create large quasi-rigid and lightweight space structures. There are numerous applications for a tethered Coulomb structure ranging from interferometry and remote sensing to component deployment and inflatable structures. This paper presents the first results of the impact of nodal attitude motions on the structure's dynamics and required charge levels. Non-linear numerical simulations analyze the complex and coupled relative motion, while analytical natural frequency expressions are developed for small deflections. Quantitative analysis shows that increasing the inflationary Coulomb forces can stiffen the entire structure to resist deformations. It is shown that for realistic charge levels the tethered Coulomb structure maintains both shape and taut tethers. This is demonstrated on a two-node system subject to initial angular rate errors and differential solar radiation pressure. Further, a simple double-tether system is shown to offer increased stiffening properties and resistance to perturbations.

Nomenclature

a, b, c	=	generic functions
A_{braid}	=	tether braid cross sectional area (m ²)
A_s	=	reflective surface area (m ²)
α	=	rotational oscillatory motion amplitude factor (N ^{1/2})
α_{10}	=	rotational oscillatory motion amplitude factor for 10 m separation (N ^{1/2})
C_R	=	surface reflectivity constant
E	=	modulus of elasticity (Nm ⁻²)
F_c	=	Coulomb force (N)
F_s	=	tether spring force (N)
F_{SRP}	=	solar radiation pressure force (N)
i	=	node index
I	=	mass moment of inertia (kgm ²)
k_c	=	vacuum Coulomb constant (Nm ² C ⁻²)
k_s	=	tether linear spring constant (Nm ⁻¹)
k_{s10}	=	nominal spring constant for 10 m separation (Nm ⁻¹)
L_e	=	tether length (m)
δL	=	tether stretch from nominal (m)
L_e	=	equilibrium tether length (m)
L_o	=	nominal tether length (m)
λ_d	=	debye length (m)
m	=	node mass (kg)
P_{SR}	=	solar radiation pressure (Nm ⁻²)
ϕ	=	double-tether attachment point half angle (rad)
q	=	node charge (C)
Q	=	combined charge product (C ²)
r	=	node spherical radius (m)
θ	=	node angular rotation (rad)
V	=	node voltage (V)
ω_T	=	translational motion natural frequency (rads ⁻¹)
x	=	node separation (m)
δx	=	increase in node separation from equilibrium (m)
x_e	=	node equilibrium separation (m)
x_o	=	node nominal separation (m)

I Introduction

The use of spacecraft for remote sensing, interferometry, and telescopic operations is a growing area of research with large baselines sought to increase power, sensor accuracy and resolution. Large space structures and free-flying spacecraft formations are two active development approaches to address this need.

Large space structures offer a rigid and fixed configuration producing a precise sensor array platform for highly accurate observations. However, there are challenges to overcome prior to large space structures becoming standard operating systems, including large mass, volume and cost constraints to get to orbit, the need for on-orbit construction or complexities and reliability of deployable components. Inflatable and deployable systems can offer a low-mass, high mechanical packaging efficiency and potentially low cost solution that can be used for applications such as antennas and booms.^{1,2,3} An ongoing area of research is the development and test of deployable components and material membranes for large space structures.⁴

An alternate method of providing the same characteristics of a large space structure is to use a cluster of spacecraft flying in a desired formation. The proposed NASA Goddard Stellar Imager⁵ and the NASA JPL study on the proposed Terrestrial Planet Finder (TPF)⁶ are two missions that intend to operate a formation of spacecraft creating a sensor baseline in the kilometer range. One of the leading applications of a large space interferometer is observations from Geostationary Earth Orbit (GEO). A study by Wertz of a GEO-based free-flying formation indicates that an Earth surface resolution of 0.5-2 m is achievable.⁷ The Eyeglass concept is another investigation into a GEO-based Earth surveillance platform with a 25-100 m aperture telescope. The diffractive lens is designed to be folded in a sequence similar to an origami layout and will be deployed in orbit.^{8,9} King and Parker in Reference 10 investigate the use of Coulomb forces to control a free-flying formation of spacecraft to develop a 20-30 m size array for interferometry at GEO.

One of the biggest challenges of a free flying formation in Earth orbit is controlling the non-linear and strongly coupled relative orbits and achieving the desired cluster geometry. With the use of conventional chemical thrusters there is a limitation of propellant and consequently mission lifetime to maintain a desired formation. With close formations and sensitive instrument missions there are also plume impingement concerns. Two formation control concepts mitigating high fuel expenditure and plume impingement are electromagnetic¹¹ and flux pinning, both of which require high operational power levels.¹² Coulomb thrust is a recent and novel method to control the separation distance of spacecraft operating in close formations that does not have plume impingement concerns, is virtually propellant-less, and requires only Watt-levels of power.^{10,13,14}

One potential solution to achieving a low-mass large space structure is with the Tethered Coulomb Structure (TCS) concept proposed in Reference 13. The TCS provides a hybrid combination of features from space structures and free flying spacecraft formations. The TCS concept utilizes a formation of spacecraft nodes that are held together with a 3D network of light-weight physical tethers. This is in contrast to other Coulomb spacecraft research

*Graduate Research Assistant, Aerospace Engineering Sciences Department, University of Colorado, Boulder, CO. AIAA student member.

†Associate Professor, H. Joseph Smead Fellow, Aerospace Engineering Sciences Department, University of Colorado, Boulder, CO. AIAA Associate Fellow

Presented as Paper 06-3792 at the AIAA Guidance, Navigation and Control Conference, San Diego, CA, July 29-31, 1996. Copyright ©1996 by the authors. Published by the American Institute of Aeronautics and Astronautics, Inc. with permission.

which investigates the use of virtual tethers using electrostatic forces.^{15,16} With the TCS concept each spacecraft node has the ability to increase its electrostatic potential through the use of a charge control device that emits either electrons or low mass ions. With each node having the same charge polarity they will repel from each other and induce a tensile force on each tether. This Coulomb repulsive force essentially inflates the spacecraft structure while the shape and size is maintained by the tethers. An illustration of a four node TCS is shown in Figure 1.

The TCS concept offers a number of advantages for the development of large space structures. Costs are kept low by launching the formation in a compact configuration that is inflated in orbit using the Coulomb forces. Similarly, a deployable component or antenna could essentially be inflated and held quasi-rigid from the spacecraft body using Coulomb force repulsion. Due to the micro- to milli-Newton levels of Coulomb force it is only necessary to have a network of small membrane-like tethers. This significantly reduces the TCS mass compared to traditional structural components and does not require on-orbit construction. It is also envisioned that structures as large as hundreds of meters are feasible by connecting multiple charged nodes with relative short and thin tethers (tens of meters). Another key benefit of the concept is its ability to vary the shape and size of the TCS configuration by varying the tether lengths. This allows adaptability and variation for changing mission requirements.

There exists a variety of applications for space tether systems and studies typically utilize a spinning system,^{17,18} a gravity gradient or an atmospheric drag orientation to maintain tension.^{19,20} A unique advantage of the TCS concept is that tension is provided with Coulomb forces regardless of the orbital orientation and can be used to overcome differential gravitational accelerations and external perturbations.

Controlling a free-flying spacecraft formation with Coulomb forces or traditional methods is an interesting dynamical challenge. On going research in this field includes equilibrium conditions of Coulomb craft,^{21,22} implementation of feedback stabilized virtual Coulomb structures with two craft,^{23,15,16} and the control of three craft.^{24,25} The navigational and dynamical motion complexities of operating tightly controlled free-flying formations are significantly simplified with the TCS concept.

The TCS concept, with its many advantages, still requires further research to address the challenges; such as low-tension tether dynamics and deployment mechanisms, the dynamics of charged quasi-rigid structures with independently rotating nodes and variable TCS shape goals, the electrical power requirements to maintain non-equilibrium charge levels, as well as the ability to maintain a delicate TCS structure during orbital maneuvers such as semi-major axis corrections. The intent of this paper is to investigate how increased nodal charge reduces attitude motions through enhanced rotational stiffness and the associated surface potentials required. The concern is that a node rotation due to small deployment errors, external torques or differential perturbations could cause the tethers to wind up or loose tension. This is an advancement over the previous TCS modeling that used point mass nodes (ignoring nodal attitude motions) and focused on how the overall structure motion and shape changes can be used to stabilize the TCS orientation.¹³

Results are generated by numerically simulating the full non-linear equations of motion for any general three-dimensional TCS size or shape using any number of spacecraft nodes. This algorithm development is shown in the Appendix. The presented research results are a vital step for the future analysis of more complex systems and higher fidelity modeling of the TCS relative motion.

Throughout this study one core aspect is determining the conditions that cause periodic slack tethers. Of interest is the amount of tether slackness that occurs with nominal configurations. It is desired that tethers do not reach a sufficiently slack state to cause tether damage or interference between nodes. However, the presence of slightly slack lines during short-term oscillations are not a strong concern.

The primary focus of this study is quantifying the ability of the Coulomb force to stiffen the overall TCS structure and resist deformation. To meet this objective, firstly, a study of the forces

acting on a TCS system at GEO is given. A two-node numerical simulation is used to explore the capability of using charge to resist compression from differential external disturbance forces. The same two-node setup is then used to demonstrate the complex 3D non-linear motions that are anticipated.

The equations of motion of this two-node system are reduced to two degrees of freedom (2DOF). This system is linearized to isolate translational and rotational motions and analysis of the natural frequencies is conducted. This gives a measure of the rotational stiffness and the effects of varying model parameters.

Numerical simulations are then used to quantify the systems ability to resist initial angular rate errors. These non-linear simulations feature dynamic tethers modeled as simple, mass-less, proportional and undamped springs. Further, to enhance the orientational stiffening capabilities of the Coulomb inflationary force, a TCS configuration with a redundant double-tether connection is investigated. This includes development of a 2DOF model and linearization analysis as well as comparing rotational stiffness to the single-tether system through numerical analysis.

II Tethered Coulomb Structure Forces

This section develops the fundamental forces acting on a TCS system. The dynamic model considered includes translational and rotational degrees of freedom of each TCS node, Coulomb forces for inflation, and fixed, deployed tether lengths to maintain a constant average size and shape. The TCS shape will undergo small variations due to flexing of the tethers and motion of the nodes. The complex coupled motions of a representative two-node TCS system are highlighted with an example simulation.

II.A Coulomb Force

The Coulomb force is the controllable actuator for the TCS system. This force is generated from the interaction of two charged bodies. The charge can either occur naturally from the space plasma, or be driven by a charge control device which continually emits charged particles. In space, the Coulomb force is reduced by shielding from the free-flying charged particles of the local plasma. The extent of this shielding is characterized by the Debye length λ_d .²⁶ The resulting space Coulomb force F_c that is generated between two craft of charges q_1 and q_2 is defined by:

$$|F_c| = k_c \frac{q_1 q_2}{x^2} e^{-x/\lambda_d} \left(1 + \frac{x}{\lambda_d} \right) \quad (1)$$

where x is the spacecraft separation distance and $k_c = 8.99 \times 10^9 \text{ Nm}^2\text{C}^{-2}$ is the vacuum Coulomb constant. The Debye length is based on the temperature and density of the local plasma. At GEO the plasma is sufficiently hot and sparse to generate Debye lengths ranging from 80 -1000 m with an average of approximately 200 m.¹⁰ This allows the use of Coulomb thrust when operating with spacecraft separations of dozens of meters at GEO.^{14,27} Low Earth orbit Debye lengths are typically cm level, making the use of Coulomb thrust challenging.

For TCS applications, the Coulomb force is chosen to be repulsive to provide an inflationary force to maintain tension on the tethers. This is achieved through a positive charge product, $Q = q_1 q_2$, with either both positive or negative q_i values. This study uses spherical spacecraft bodies where a charge level q requires a surface potential computed with the relationship:

$$q = \frac{Vr}{k_c} \quad (2)$$

where V is the voltage and r is sphere radius. Note that this study does not consider non-homogeneous charge distributions that can occur from induced charge effects of two neighboring conducting objects. Such effects are very small for separations greater than 5 sphere radii $x > 5r$. Also omitted from this study is the combined charge effect of having finite spheres in close proximity. The consequence is that for separations less than 10 sphere radii $x > 10r$, the craft would require a slightly higher surface potential to compensate for the minimal force reduction.

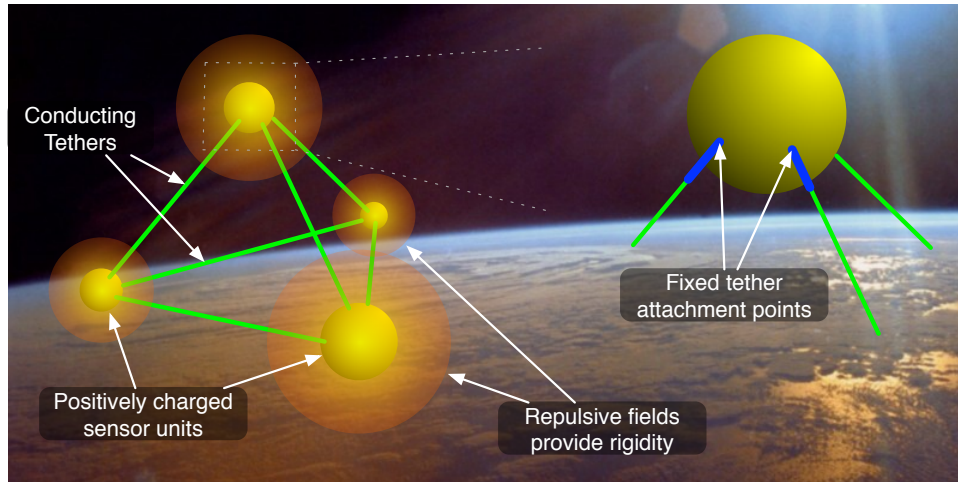


Figure 1: Illustration of the tethered Coulomb structure concept

II.B Tether Force

The tethers are modeled as linear stretch springs that, when in a compressed state, go slack and no force is produced. Consequently they only produce a force that opposes the repulsion of the Coulomb force. The magnitude of the force is governed by the equation:

$$|\mathbf{F}_s| = \begin{cases} k_s \delta L & \delta L > 0, \\ 0 & \delta L \leq 0. \end{cases} \quad (3)$$

where k_s is the linear spring constant and δL is the stretch in the tether length between two nodes. A linear spring tether is a suitable model for this study that is analyzing the relationship between translational and rotational motions with an emphasis on overall structural stiffening and disturbance rejection. The TCS algorithm is developed to allow future investigations to use more complex tether models which consider geometric deformations of the low-tension tether. However, the linear axial-stiffness model with nominal material property values provides an approximate measure of how well the two-node TCS could resist differential rotations.

One option for a spacecraft tether material is AmberStrand®^a. The property values of this reference material are used for all simulations in this paper. AmberStrand® is an electrically conductive hybrid yarn made up of a metal coated polymer that offers a flexible, low-mass and high strength tether. Tests conducted at the University of Colorado at Boulder on a braid of three twisted Amberstrand® fibers resulted in the tether properties shown in Table 1.

Table 1: AmberStrand® properties for 3 twisted fibers

Parameter	Value	Units
Modulus of elasticity (E)	9.5×10^9	N/m ²
Cross sectional area (A_{braid})	5.6×10^{-7}	m ²
Linear mass density	1.44	g/m

The modulus of elasticity is measured in the elastic region of tensile test results. The modulus of elasticity is related to a linear spring constant in the elastic region of the stress-strain curve with:

$$k_s = \frac{EA_{\text{braid}}}{L_o} \quad (4)$$

where E is the modulus of elasticity, A_{braid} is the cross sectional area of the braid of three twisted fibers, and L_o is the un-stretched tether length.

II.C Solar Radiation Pressure

At GEO, where the TCS concept is to be operated, solar radiation pressure (SRP) can play a significant role as a disturbance

force on the inertial orbital motion of satellites.²⁸ For the TCS application the primary concern here is the effect of any differential SRP forces on short-term dynamics. A simplified Solar Radiation Pressure (SRP) model is used to quantify the capability of the TCS system to compensate for a constant external perturbation. The magnitude of the SRP force acting on a spacecraft is governed by the relationship:²⁹

$$F_{SRP} = P_{SR} C_R A_s \quad (5)$$

where P_{SR} is the solar radiation pressure, C_R is the surface reflectivity constant of the spacecraft, and A_s is the surface area.

II.D Sample Force Magnitudes

To appreciate the expected force magnitudes a TCS structure will encounter on orbit, consider a two-node tethered system. With nodes of radius 0.5 m, separated by 5 m center to center and charged to a surface potential of 30 kV the expected force levels are shown in Table 2. This is an achievable charge level. SPEAR-1 demonstrated controlled charge to 46 kV.^{30,31} The Coulomb force is computed between two isolated point charges. The solar radiation pressure is computed for one node at 1 Astronomical Unit (AU) from the sun where the solar radiation pressure is 4.56×10^{-6} N/m, and the surface reflectivity is 1. The differential gravity gradient force is computed assuming the nodes are aligned along the nadir line at GEO altitude, each with a mass of 50 kg.

In the absence of external perturbations (such as SRP or gravity gradients) there exists a force equilibrium between the Coulomb and tensile forces. For two nodes at 30 kV potential, with a desired separation ($x_o = 5$ m), and using Amberstrand® tether material need only stretch $0.75 \mu\text{m}$ to reach this equilibrium separation (x_e).

Table 2: Expected force magnitudes for a two-node TCS separated by 5 m

Force	Value	Units
Coulomb (F_c)	1.0	mN
Tether (F_s)	1.0	mN
SRP (F_{SRP})	3.6	μN
Differential gravity	4.0	μN

II.E Numerical Simulation: TCS Compression Due to External Disturbance Force

The force magnitudes of the primary disturbances at GEO, differential SRP and differential gravity, are three orders of magnitude less than the Coulomb control forces. The intent of the following study is to quantify the capabilities of a two-node TCS configuration to resist deformation from an external perturbation, in this case, differential SRP.

Consider two spacecraft nodes connected with a single-tether. The solar radiation pressure is added as a bias force that is compressing the system along the direction of the tether line as shown

^aSyscom Advanced Materials, Inc. www.amberstrand.com, 1/15/2010

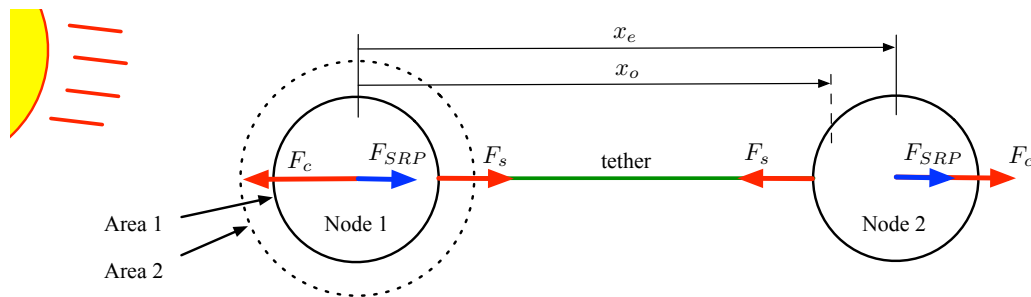


Figure 2: Two-node Solar radiation pressure model

in Figure 2. The SRP force is acting on both nodes, but increasing the size of node 1 produces a differential SRP that attempts to compress the nodes. The concern is whether the Coulomb forces are large enough to maintain tether tension in this setup. The parameters of the study are shown in Table 3 and the simulation algorithm used is shown in the Appendix.

Table 3: Case 3 Simulation Parameters

Parameter	Value	Units
Spacecraft Area Ratios	1-10	
Spacecraft node radius (r)	0.5	m
Spacecraft separation (x_o)	10	m
Solar pressure (1 AU)	4.56×10^{-6}	Nm^{-2}
Surface reflectivity	1	

The nodes are separated by 10 m. If the Coulomb forces are found to be sufficient to maintain tension for this challenging larger separation distance, then TCS systems of shorter separation distances should not be significantly compressed by differential SRP. The sunlit surface area of node 1 is increased linearly in multiples from one to ten, where one is the nominal surface area corresponding to a 0.5 meter radius circle. An increase in the surface area will cause the homogeneously distributed charge to also increase for a fixed nodal potential. This would further increase the stiffening capabilities of the TCS system. To maintain a worst-case scenario, this model does not incorporate any change in the Coulomb force as the surface area of node 1 is increased. To isolate the differential solar radiation pressure effects, this simulation is setup to not induce attitude rotations and omits gravity forces.

The numerical simulation is set up with the craft initially at their undisturbed equilibrium states. The contour plot of Figure 3 shows what the worst-case percentage of the buffer between equilibrium distance and un-stretched distance is compromised by the SRP disturbed relative motion. This value is calculated using:

$$\% = \frac{L_e - \min(L)}{L_e - L_o} 100 \quad (6)$$

This percentage value indicates how close the tether length is from becoming slack as a function of both charge and the surface area ratio between the craft. The top left portion of the figure indicates that the crafts relative motion compresses to the point of causing the tether to go slack at times.

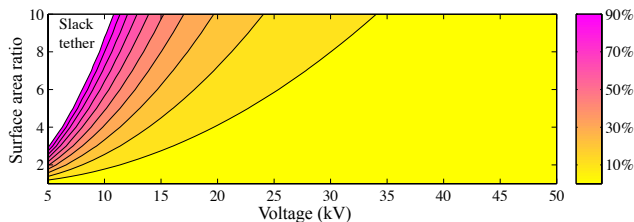


Figure 3: Tether distance from becoming slack under varying SRP disturbances

As indicated in Figure 3 an increase in charge will stiffen the system to resist differential perturbations. For shorter separation distances of less than 10 meters the system is further stiffened

reducing the voltage requirements to resist the same disturbance force levels. Note that even with a very large TCS node size ratio of 10 and 25 kV potential, the compression due to this worst-case alignment of the differential SRP disturbance would only cause approximately a 20% compression of the equilibrium distance buffer. For TCS separation distances on the meter-level, considering near equal nodal sizes, the differential SRP will have a minimal impact on the TCS shape. Based on the results of this simulation it is appropriate to omit the effects of differential perturbations such as SRP and gravity to analyze short-term dynamical motions. For long term dynamic studies, that are not performed here, the implementation of the full model in the appendix is used.

III Two-Node Simulation Parameters

The intent of this paper is to provide insight into the dynamics and design parameters of the TCS concept. These studies are based upon the translational and rotational motion of a representative two-node system. The two-node system is subjected to initial angular rate errors that represent deployment or disturbance torques.

Simulations are computed with the full three-dimensional equations of motion including attitude dependence, as detailed in the Appendix. For practical reasons, the simulations are stopped if an attitude reaches a tether wrap up state (± 90 degrees for single-tether). A common set of TCS parameters for each simulation case is shown in Table 4. The three un-stretched separations of $x_o = 2.5, 5,$ and 10 m are measured from node center to center.

Table 4: Simulation Parameters Common For All Test Cases

Parameter	Value	Units
Spacecraft node mass (m)	50	kg
Spacecraft node radius (r)	0.5	m
Spacecraft potential range (V)	5-50	kV
Spacecraft separations (x_o)	2.5, 5, 10	m
Initial attitude rate errors ($\dot{\theta}(0)$)	1-120	deg/min

To demonstrate the complex coupling between translational and attitude motions of tethered, charged nodes an example simulation is shown. Figure 4 shows the relative motion of a two-node system in deep space. Each node has an initial angular rate of 45 deg/min about different axes. The nodes maintain a fixed potential of 30 kV and there are no gravity or SRP forces acting. The nodes have an un-stretched separation of 5 m, radius of 0.5 m and mass of 50 kg. Figure 4 demonstrates the relative oscillatory motion of the two nodes along with attitude of node 1 and the corresponding tether force levels.

Figure 4 indicates the complex dynamics that result from a two-node, single tether TCS system under the influence of solely an initial angular rate. While this numerical simulation can handle general translational and rotational motion of N nodes, the results yield an overwhelming amount of data, making it difficult to gain any insight. This numerical demonstration highlights the need to reduce the complexity of the system. It is beneficial to isolate the motions of the TCS system and appreciate its true capabilities. For this reason, the following studies in this paper reduce a generic TCS system to its fundamental translational and rotational motions.

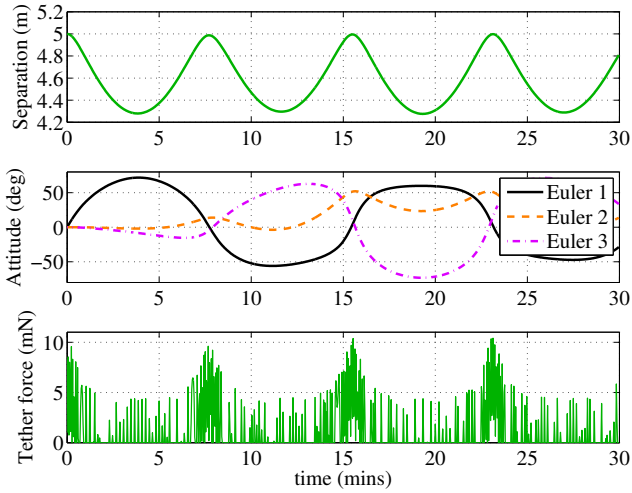


Figure 4: Complex 3D example of a two-node relative motion, attitude and single-tether tension (initial angular rates of 45 deg/min)

IV Single-Tether Configuration Modeling

This section documents the dynamic model of a representative two-node, single-tethered TCS system. This two-node model is reduced to two degrees of freedom and linearized to obtain insight into expected motions about equilibrium. The linearization allows specific analysis of individual translational and rotational motions. The models are developed in this section in the absence of gravitational and solar radiation pressure perturbations. The two-degree of freedom models developed here also provide verification of the full 3D model and simulation results.

IV.A Two Degree of Freedom Model

A simplified two degree of freedom TCS model is developed to provide insight into how TCS node rotation impacts the charge requirements and related stiffness capabilities. This TCS model features two nodes attached with a single-tether as shown in Figure 5.

By constraining the nodes to asymmetrically rotate by an angle θ the tether remains parallel to the line of sight vector resulting in one dimensional translational motion with the Coulomb and Tether forces (F_c & F_s) directly opposing each other. This reduces the model to one rotational degree of freedom and one translational. This motion is desirable as it allows analysis of the effects of each motion in isolation. Any alternate symmetries cause two dimensional translational motions that are also inherently coupled to rotational motions. The Coulomb force for this model is assumed to have no shielding from the plasma environment due to the very small meter-level separation distances. This is a reasonable assumption given the force magnitude is reduced only 0.03% at a separation of 5 meters in a nominal 200 m Debye length plasma.

The translational equation of motion of this system is:

$$\ddot{x} = \frac{2k_c Q}{m x^2} - \frac{2k_s}{m} [x - x_o + 2r(1 - \cos \theta)] \quad (7)$$

where x_o is the un-stretched node separation and m is the node mass. With the tethers attached at fixed locations on the spherical surfaces any rotation will result in a torque on the node. This is modeled to examine the correlations between translational and rotational motions. The attitude is governed by the rotational equation of motion:

$$\ddot{\theta} = -\frac{r k_s}{I} [x - x_o + 2r(1 - \cos \theta)] \sin \theta \quad (8)$$

where I is the mass moment of inertia of the node. For this 2DOF model the mass of each node is equal and the mass moment of inertia of a solid disk is used. Future studies can vary these properties to analyze the effect of mass and its distribution on the dynamics of the system.

IV.B Single-Tether Linearized model

To focus on the dynamical motion of the nodes, the 2DOF model is linearized. Equation (7) has an equilibrium condition at a separation, $x = x_e$ and an attitude $\theta = 0$. At this equilibrium, the translational equation of motion is reduced to

$$\ddot{x} = 0 = \frac{k_c Q}{x_e^2} - k_s (x_e - x_o) \quad (9)$$

which can be arranged to a cubic relationship between the equilibrium distance x_e and the associated charge product Q :

$$k_c Q = k_s (x_e - x_o) x_e^2 \quad (10)$$

Of the three x_e solutions only the real solution is practical. At this equilibrium separation distance the Coulomb and tether forces are equal and the nodes remain stationary (with no external disturbances). One interesting consequence of this equilibrium distance is that it is independent of the system mass.

The 2DOF model given in Eqs. (7) and (8) is linearized about the equilibrium condition to produce a reduced system model to study the dynamic behavior of oscillations about the equilibrium states. Linearizing the translational motion for small departures ($\delta x = x - x_e$) results in:

$$\delta \ddot{x} \approx -\frac{2}{m} \left[\frac{2k_c Q}{x_e^3(Q)} + k_s \right] \delta x \quad (11)$$

This approximate translation description is decoupled from the angular rotation and is the form of the stable, undamped harmonic oscillator equation. The natural frequency of this oscillatory translational response is given by:

$$\omega_T = \sqrt{\frac{2}{m} \left[\frac{2k_c Q}{x_e^3(Q)} + k_s \right]} \quad (12)$$

The rotational equation of motion is linearized to the form:

$$\ddot{\theta} \approx \frac{-r k_s}{I} [x_e(Q) - x_o] \theta \quad (13)$$

This linearized rotational equation of motion also decouples and is of the form of the stable undamped harmonic oscillator equation. The natural frequency of this oscillatory rotational response is given by:

$$\omega_R = \sqrt{\frac{r k_s}{I} [x_e(Q) - x_o]} \quad (14)$$

While these linearized models are only valid for small oscillations, they can be used to offer insight into the response of the system about its equilibrium state.

V Linearized Model Analysis

Using the linearized system model, two case studies are used to analyze motions and sensitivity to nodal parameters. Ultimately, it is possible to gauge the expected stiffness of the TCS, with the linearized models of Equations (11) and (13) and the system properties of Table 4.

V.A Natural Frequency Response

The natural frequency of the linearized translational and rotational motions of Equations (12) and (14) gives a measure of the TCS stiffness. Figure 6 shows the natural frequency of the linearized translational motion for three separation distances. For the voltage range analyzed, the natural frequency of the response changes less than 0.1%, indicating that it is essentially independent of the spacecraft charge. The translational stiffness is largely determined by the tether material stiffness. As the separation distance between the nodes decreases, the frequency of the system response increases as a result of the shorter (stiffer) tethers and enhanced Coulomb force magnitudes.

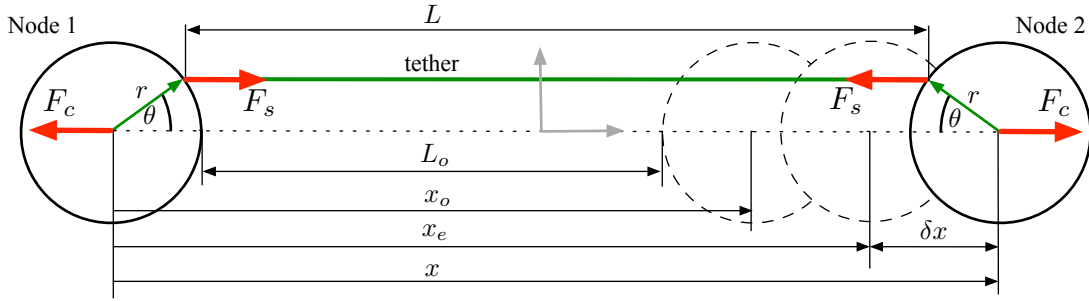


Figure 5: Two-node system showing two degree of freedom motion through asymmetric rotations

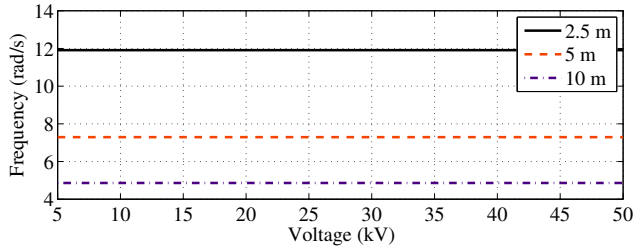


Figure 6: Natural frequency of linearized translational motion

Figure 7 shows the natural frequency of the linearized rotational motion, Equation (14), for three separation distances. In contrast to the translational stiffness which is essentially decoupled from the magnitude of the electrostatic inflation force (assuming AmberStrand®-like materials), the rotational stiffness or natural frequency is directly related to the TCS node potentials. The rotational natural frequency has a near-linear dependence on potential for the range of charges used in this study. In essence, the rotational motion will be stiffened through enhanced charge levels. Only for potentials much larger and unrealistic for spacecraft charging (>2000 kV) does the response become non-linear.

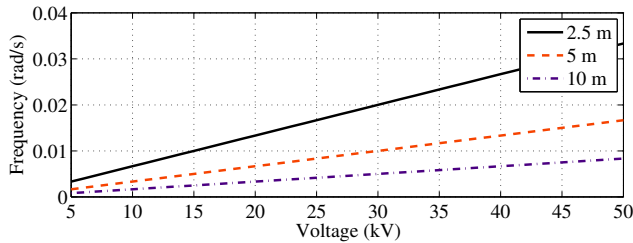


Figure 7: Natural frequency of linearized rotational motion

Note that the translational natural frequency is at least two orders of magnitude greater than the corresponding rotational motion. For these uncoupled linearized equations and the system parameters analyzed this implies that a TCS is naturally superior at constraining translational motion. Based on this outcome, the primary focus of this study is on the nodal rotational responses.

V.B Sensitivity of Rotational Motion to Tether Material

AmberStrand® is the example tether material used for this study. The use of an alternate tether material would change the material stiffness (spring constant). The linearized model is used to analyze the effect on the resulting rotational node motion by varying this tether material stiffness. Equation (13), which is the form of a stable oscillator, has the solution $\theta(t) = A \sin(\omega_R t + \beta)$ where β is the phase offset and the amplitude of the rotational response oscillation, A is defined as:

$$A = \dot{\theta}(0) \sqrt{\frac{2mr}{5}} \underbrace{\sqrt{\frac{1}{k_s(x_e(Q, k_s) - x_o)}}}_{\alpha} = \dot{\theta}(0) \sqrt{\frac{2mr}{5}} \alpha \quad (15)$$

Here $\dot{\theta}(0)$ is the initial angular rate and $\theta(0)$ is assumed to be

zero. The amplitude A is proportional to α , which is a function of the tether stiffness k_s and node charge product Q . Note that x_e depends on k_s so amplitude is not inversely proportional to the spring constant. For 10 m separated nodes tethered with the nominal AmberStrand® braid the resulting spring constant value is $k_{s10} = 591$. This spring constant value corresponds to an amplitude factor α_{10} . This study investigates the impact of a range of material properties on the rotational stiffness. This is performed by varying the spring constant value from $k_{s10} \times 10^{-8}$ through $k_{s10} \times 10$. The resulting amplitude multiplication factor α of Equation (15) is normalized by the nominal α_{10} value and plotted in Figure 8.

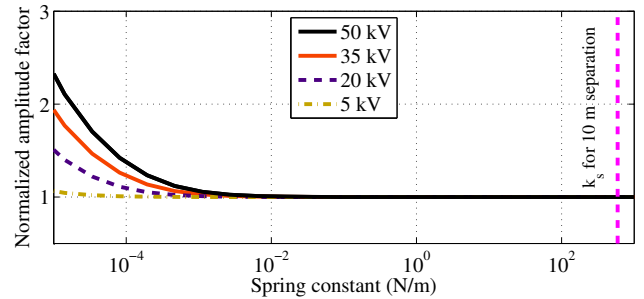


Figure 8: Effect of varying tether spring constant on the amplitude of linearized angular oscillations

This study indicates that changes in the tether spring constant have a minimal effect on the amplitude of angular rotations compared to the nominal 10 m separation (k_{s10}) response. It requires a spring constant that is reduced by 1×10^{-8} times the value of the 10 m separated case and nodes of 50 kV to increase the maximum angular rotation by only 2.5. Any tether material with a realistic spring constant or anything stiffer than the example tether material will result in the same rotational motion response, an important finding of the linearized analysis.

V.C Extent of Linearization Range

The previous section used linearized equations to analyze expected motions about equilibrium conditions. Numerical simulations using the 2DOF equations are used to quantify the extent of accuracy of these linear approximations. This is achieved by calculating the period of oscillation of the system response to deviations from equilibrium both with the translational and rotational equations of motion.

Figure 9 shows the period of oscillation of the two-node system initialized with a translational offset δx from equilibrium x_e . The period of oscillation is compared to that predicted from the linearized system of Equation 12. The nodes are offset in both the compression and stretch directions ($x_e \pm \delta x$) and give different periods of oscillation. This figure indicates that the range of accuracy of the linearized translational equation is only $\pm 1 \times 10^{-3}$ mm.

Similarly, the period of oscillation of the two-node system initialized with a rotational offset $\delta \theta$ from the equilibrium angle of zero is shown in Figure 10. The period of oscillation is compared to that predicted from the linearized system of Equation 14. Due to symmetry the nodes are offset only in the positive θ direction. This figure indicates that the range of accuracy of the linearized rotational equation is $\pm 8 \times 10^{-2}$ degrees. Beyond this linear range

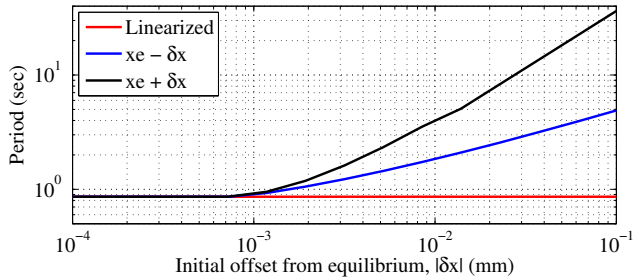


Figure 9: Comparison of oscillation periods for linearized translational equation to non-linear simulation

the rotational oscillations abruptly change periods as the tether now becomes marginally slack at times causing the nodes to lose their smooth rotations.

The conclusion of this study is that the linearization analysis only holds for very small departures from the respective equilibriums. The non-linear nature of the TCS dynamics dominate, leading to the need for numerical simulations for further analysis.

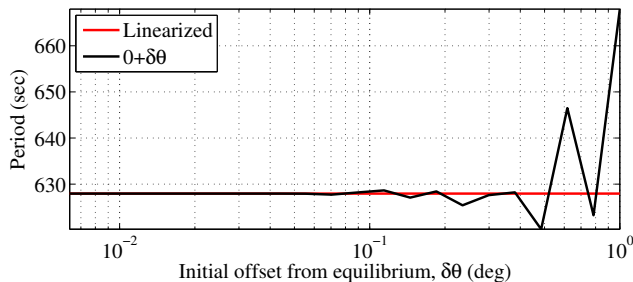


Figure 10: Comparison of oscillation periods for linearized rotational equation to non-linear simulation

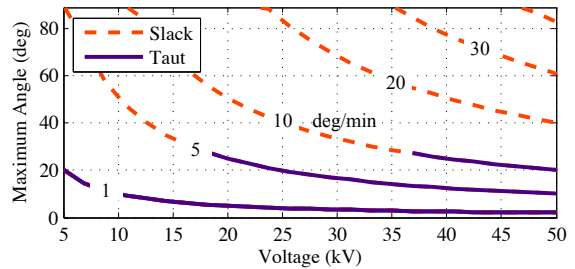
VI Numerical Simulation: Rotational Stiffness Capabilities

The linearized analysis gave an indication of the translational and rotational motions and their dependence on two key system parameters, craft potential and tether material. Due to the very non-linear nature of TCS dynamics, further analysis of the rotational motion is conducted to demonstrate the TCS stiffening properties and capability to resist angular rate errors.

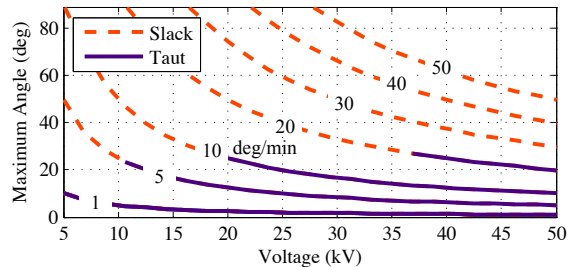
After deployment the TCS nodes will not be perfectly at rest with respect to each other. This analysis uses the full 3D non-linear equations of motion (see Appendix) to demonstrate the ability of the Coulomb force to stiffen the structure and resist deformation due to a small initial angular rate. Three two-node, single-tether configurations of different separation distances are simulated with asymmetric initial angular rotations. Here both nodes perform the same (but opposite) rotation and consequently have one dimensional translational motion, to focus on rotational dynamics.

Figure 11 shows the maximum attitude angle that is reached by the nodes for each of the separation distance cases. This is shown as a function of the spacecraft surface potential and each data line corresponds to the initial angular rate error. No material damping is considered in this study as the focus is on the initial rotational response and issues with tethers wrapping up on nodes after a single oscillation. The weak material damping would only impact long-term oscillation amplitudes.

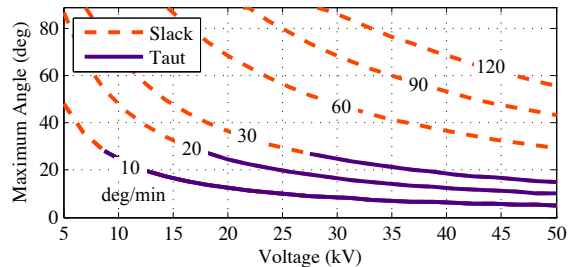
The solid lines in Figure 11 indicate that the tether remains taut for the simulation duration, where as the dashed regions have the tether reach a slack state. For many of these conditions the tether may go slack only a small fraction of the simulation time and is typically much less than a millimeter from the un-stretched tether length. Given that there are only infrequent times of slight slackness, this is not a significant concern. It is anticipated that passive or active damping be added to the TCS system to assist the transient response to reach a taut tether equilibrium state. Future research investigating the use of active motion damping or passive damping with viscous materials at the tether attachment points is envisioned.



a) Maximum angle for 10 m separated nodes



b) Maximum angle for 5 m separated nodes



c) Maximum angle for 2.5 m separated nodes

Figure 11: Maximum attitude reached as a function of initial attitude rate error

For the three separation cases analyzed the conditions that cause the angle of rotation to go above 27° results in a tether that will periodically go slack. Interestingly this rotation amplitude limit appears to be independent of the initial conditions considered or the node separations. The cause of this correlation is currently unknown and under investigation.

A reduction in the spacecraft separation distance results in two key changes on the system as shown in Figure 11. Firstly, the tether spring constant increases and secondly the spacecraft will be closer together, increasing the Coulomb force for an equivalent charge level. This increases the stiffening of the rotational motion, as precluded by the earlier linear analysis. This simulation now quantifies the enhanced ability of a stiffened TCS to resist deformation due to an initial angular rate error on the nodes. Figure 11(a) shows that a 10 meter nodal separation with 35 kV potentials requires an initial nodal rotation rate less than 10 deg/min, a small value. Otherwise, the tethers will periodically go slack, or the nodes could wrap up with the tethers. In contrast, Figure 11(c) shows that reducing the separation to 2.5 m and maintaining a 35 kV potential will constrain a 45 deg/min angular rate. At these separations rates as high as 120 deg/min can be tolerated without nodal wrap up. Shorter separation distances yield significant increases to the rotational stiffness of the TCS nodes.

VII Double-Tether Rotational Stiffness Capabilities

Having a TCS system that incorporates a redundant set of tethers between the nodes, with the attachment points distributed across the nodes surface, is a method of increasing the rotational TCS node stiffness. The following numerical simulation results quantify

by how much the rotational TCS node stiffness can be increased if a double-tether setup is employed.

VII.A Two Degree of Freedom Model

The double-tether TCS concept is shown in Figure 12 on a two-node system. The intent of the redundant double-tether is to add rigidity and resistance to deformation for the TCS. The system is modeled with asymmetric motions so that it can once again be reduced to two degrees of freedom to gain analytical insight.

The translational equations of motion of the symmetric double-tether system is:

$$\ddot{x} = \frac{2k_c Q}{m x^2} - \frac{4k_s}{m} [x - x_o + 2r \cos \phi (1 - \cos \theta)] \quad (16)$$

where ϕ is the half angle between the tether attachment points. The rotational equation of motion is given by:

$$\ddot{\theta} = -\frac{2rk_s \sin \theta}{I} \left\{ \cos \phi (x - x_o) + 2r \left[\cos \theta + \cos^2 \phi - 2 \cos \theta \cos \phi \right] \right\} \quad (17)$$

The rotational equation of motion is significantly more complex than the single-tether setup. However, linearizing the double-tether motions about the equilibrium states, still produces a decoupled set of equations. The translational motion for small departures about the equilibrium ($\delta x = x - x_e$) is:

$$\delta \ddot{x} \approx -\frac{4}{m} \left[\frac{k_c Q}{x_e^3(Q)} + k_s \right] \delta x \quad (18)$$

This linearized translational motion is of the form of a stable undamped harmonic oscillator. It is also equivalent to the single-tether case of Equation (11) with an additional factor of two. This further increases the natural frequency and stiffness of the translational response. The rotational equation of motion is linearized to the form:

$$\ddot{\theta} \approx \frac{-2rk_s}{I} [(x_e(Q) - x_o) \cos \phi + 2r(1 - \cos^2 \phi)] \theta \quad (19)$$

This linearized rotational equation of motion decouples from the translational motion and is a stable undamped harmonic oscillator equation. Unlike the single-tether rotational motion of Equation (13) this linearization features dependance on the tether attachment angle ϕ . Figure 13 plots the rotational natural frequency of Equation (19) as a function this tether attachment angle and potential. This figure shows how stiffening is significantly increased with the tether angle ϕ . This geometric stiffening is a consequence of the larger moment arm acting on the node. The data in this figure is generated with nodes of 0.5 m radius separated by 2.5 m. It should be noted that with zero tether separation ($\phi = 0$) the double-tether rotational natural frequency is equivalent to the single-tether system shown in Figure 7.

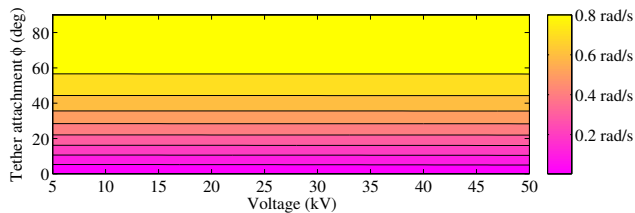


Figure 13: Natural frequency of linearized rotational motion of double-tether model

Figure 7 showed for the single-tether case that increasing charge increases the natural frequency of the rotational response. This also occurs with the natural frequency of the double-tether shown in Figure 13, however has less contribution than the geometric stiffening. Utilizing a double-tether will increase the ability to resist nodal angular rotations.

VII.B Double Tether System Response to Angular Rate Errors

In this simulation case the double-tether response to angular rate errors is compared to that of a single-tether configuration. A two-node configuration with a separation of 2.5 m is analyzed. The simulation is performed using the full 3D and non-linear coupled equations of motion. The parameters of the symmetric simulation are shown in Table 5.

Table 5: Double Tether Simulation Parameters

Parameter	Value	Units
Initial attitude rate errors ($\dot{\theta}(0)$)	5,10	deg/min
Spacecraft node radius (r)	0.5	m
Spacecraft separation (x_o)	2.5	m
Tether attachment point angle (ϕ)	20	deg

Using two initial angular rate errors for each tethered system the resulting maximum attitude angle reached is shown in Figure 14 on a y-axis log plot. There is a noticeable difference in the systems responses. The double-tethered system performing better at reducing maximum rotation due to initial rate errors. This indicates that the resulting moment arm from the double-tether configuration significantly increases the system's response to angular rates. While the double-tether system has the advantage of producing a stiffer system, it is also prone to having a tether go slack as shown by the dashed lines in the figure. The tether is only marginally and momentarily slack at times of closest approach between the nodes. Once again, during these times the tether is slack less than 1 mm over its entire length. In contrast, during this simulation case the single-tether system remains taut for any charge above 10 kV, at a cost of reaching higher attitude angles. Another consideration with the double-tether TCS is that the nodes are inherently closer to wrap up due to the tether connection angle. A comparison between the resistance to absolute angular rotation versus the close proximity to wrap up must be considered.

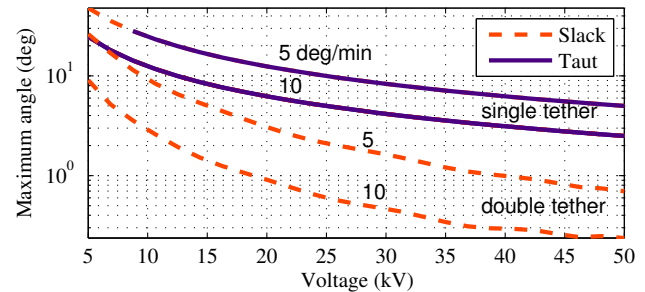


Figure 14: Double-tether vs single-tether attitude response to angular rate errors

The results of this simple double-tether simulation indicate that a TCS system can be significantly stiffened beyond an equivalent single-tether system. This offers enhanced capabilities to resist torque disturbances or deployment motions. An additional advantage is the safety provided by having two tethers between nodes. In case one tether is severed, the remaining tether would still maintain the TCS shape, although with reduced accuracy.

VIII Conclusions and Future Work

The novel TCS concept offers unique on-orbit advantages. Large space structures are envisioned that can be launched in a low-mass and compact configuration and deployed and resized once on-orbit. To advance the concept, this study analyzes the coupling between relative translational and rotational motions of the tethered spacecraft nodes. A baseline two-node TCS system is the focus of this study.

Numerical results obtained with the full three dimensional non-linear equations of motion indicate that external perturbations such as SRP or differential gravity have minimal influence on the short-term dynamics. For obtainable kilo-volt level potentials the TCS

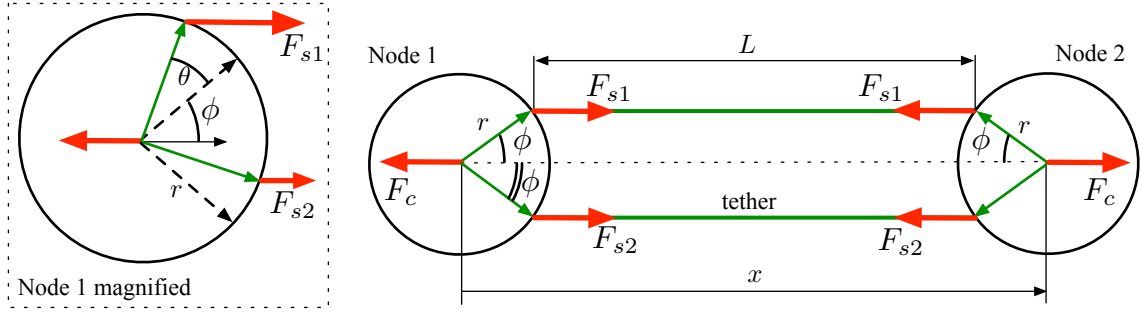


Figure 12: Two-node system with double-tether

system will sufficiently inflate and resist deformation from external forces. This is shown firstly through simplified, linearized models, that give an analytical expression for the natural frequency of isolated translation and rotational motions. The natural frequency is an indication of the stiffness of the system and the rotational motions offer lower values and are the focus of this study. The TCS rotational response to initial angular rate errors is also quantified and shown to significantly improve with the use of an additional tether.

This versatility of the numerical simulation and ability to examine any general N -node TCS system will be advantageous in future TCS studies where more complex networking is considered. This two-node study considers a worst-case situation where the tether network provides minimal rotational stiffening. Multi-tether connections to a node, such as with a three-node triangular system, will provide increased rotational stiffness. This concept is illustrated in this study by investigating the multi-tether connection among two nodes. Future studies will investigate three dimensional TCS configurations as well as incorporate low-tension behavior models.

Acknowledgements

The authors would like to thank the Aerospace Engineering Sciences senior design team, *CTS - CubeSat Tether System*, for the AmberStrand® material properties.

Appendix - Three Dimensional TCS Modeling

The simplified 2DOF TCS models offer insight into translational and rotational motion. Shown here is the development of the full three dimensional non-linear equations of motion that can accommodate general TCS spacecraft configurations. The algorithm simulates the TCS in deep space, or under the gravitational attraction of orbit and incorporates external disturbance forces, such as SRP. Although not performed in this study, the intent of this algorithm is to fully explore the capabilities and operating regimes of the TCS along with a study of its dynamic behavior under realistic disturbance environments. The algorithm can perform TCS relative motion studies accommodating any number of nodes and tethers in any initial orbit configuration.

The location of each spacecraft node, \mathbf{R}_i , is defined in an Earth centered inertial (ECI) frame. At epoch, the body frame alignment and nominal separation distances of each node is defined. The equations are shown here for nodes connected with just a single-tether that has a fixed attachment point on the spherical surfaces. It is not necessary to have a tether connecting each node as a tether connection matrix, $[K_{ij}]$, defines which nodes are connected. The tethers are modeled as linear springs and can stretch from either the nodal relative motion or from attitude rotations as shown in Figure 15. The resulting tensile force acting on node i from the tether connected to node j is:

$$\mathbf{T}_{ij} = k_s \delta L_{ij} \hat{\tau}_{ij} \quad (20)$$

where τ_{ij} is the vector defining the tether connecting node i to j . When the tether length is shorter than desired, the tether goes slack and there is no force acting on the corresponding nodes.

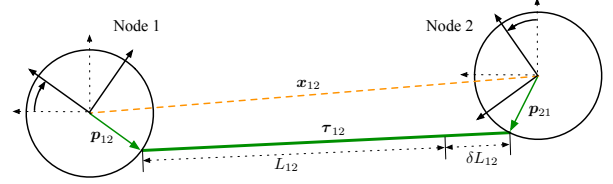


Figure 15: Two-node example of attitude change and increased tether length

VIII.A Translational Equation of Motion

Using the Coulomb force of Equation (1), tensile force and the gravitational force, the resulting equations of motion of each node is calculated using:

$$\begin{aligned} \ddot{\mathbf{R}}_i = & -\frac{\mu}{|\mathbf{R}_i|^2} \hat{\mathbf{R}}_i + \sum_{j=1}^N K_{ij} \frac{\mathbf{T}_{ij}}{m_i} \\ & + \sum_{j=1}^N \frac{k_c q_i q_j (-\hat{\mathbf{x}}_{ij})}{m_i x_{ij}^2} e^{-x_{ij}/\lambda_d} \left(1 + \frac{x_{ij}}{\lambda_d}\right) \\ & + \mathbf{F}_{SRP} \quad i \neq j \quad (21) \end{aligned}$$

where $\mu = 3.986 \times 10^{14} \text{ m}^3 \text{ s}^{-2}$ is the gravitational coefficient for Earth, m_i is the spacecraft node mass, N is the total number of nodes in the TCS model. K_{ij} is a scalar based on the adjacency matrix which is 0 if no tethers connected or 1 if any tethers are connected. Note that these charges do not influence the relative motion. They simply provide an inflating force, relative to the systems center of mass, that increases the tether tensions. In addition, the Coulomb force is calculated based on a point charge approximation, even though the nodes have a distributed surface charge. The motion of each node is propagated in time using a variable step Runge-Kutta algorithm.

VIII.B Nodal Rotational Equation of Motion

The attitude of each spacecraft node is also propagated by computing the torque acting on the node from each tether:

$${}^B \boldsymbol{\Gamma}_i = \sum_{j=1}^N \left(K_{ij} {}^B \mathbf{p}_{ij} \times [B\mathcal{I}]_i^T \mathbf{T}_{ij} \right), \quad i \neq j \quad (22)$$

Where \mathbf{p}_{ij} is the body fixed vector that defines the location of the tether connection point on node i that connects to node j and $[B\mathcal{I}]_i$ is the direction cosine matrix of the attitude of node i relative to the inertial frame. The angular acceleration of each node is defined in the body frame with Euler's rotational equations of motion:³²

$$[I] \dot{\boldsymbol{\omega}}_i = -\boldsymbol{\omega}_i \times ([I] \boldsymbol{\omega}_i) + \boldsymbol{\Gamma}_i \quad (23)$$

The attitude of each node is represented with the modified Rodrigues parameters (MRP) which are integrated using the differential kinematic equation:

$$\dot{\boldsymbol{\sigma}}_i = \frac{1}{4} \left[(1 - \sigma_i^2) [I_{3 \times 3}] + 2[\boldsymbol{\sigma}]_i + 2\boldsymbol{\sigma}_i \boldsymbol{\sigma}_i^T \right] \boldsymbol{\omega}_i \quad (24)$$

The MRP set will go singular with a rotation of $\pm 360^\circ$. To ensure a non-singular description, the MRP description is switched to the shadow set whenever $|\sigma| > 1$.³²

References

- ¹Freeland, R. E., Bilyeu, G. D., Veal, G. R., and Mikulas, M. M., "Inflatable Deployable Space Structures Technology Summary," *49th International Astronautical Congress*, Melbourne, Australia, Sept. 28 – Oct. 2 1998.
- ²Cobb, R. G., Lindemuth, S. N., Slater, J. C., and Maddux, M. R., "Development and Test of a Rigidizable Inflatable Structure Experiment," *45th AIAA/ASME/ASCE/AHS/ASC Structures, Structural Dynamics & Materials Conference*, Palm Springs, CA, April 19–22 2004, Paper No. AIAA 2004–1666.
- ³Tarazaga, P. A., Inman, D. J., and Wilkie, W. K., "Control of a Space Rigidizable Inflatable Boom Using Macro-fiber Composite Actuators," *Journal of Vibration and Control*, Vol. 13, No. 7, 2007, pp. 935–950.
- ⁴Fang, H., Knarr, K., Quijano, U., Huang, J., and Thomson, M., "In-space Deployable Reflectarray Antenna: Current and Future," *AIAA/ASME/ASCE/AHS/ASC Structures, Structural Dynamics and Materials Conference*, Schaumburg, IL, April 7–10 2008.
- ⁵Carpenter, K. G., Schrijver, C. J., Karovska, M., and Team, S. M. C. D., "The Stellar Imager (SI) Project: A Deep Space UV/Optical Interferometer (UVOI) to Observe the Universe at 0.1 Milli-arcsec Angular Resolution," *Proceedings of the NUVA Conference*, El Escorial, Spain, June 2007.
- ⁶Blackwood, G., Henry, C., Serabyn, E., Dubovitsky, S., Aung, M., and Gunter, S. M., "Technology and Design of an Infrared Interferometer for the Terrestrial Planet Finder," *AIAA Space 2003*, Long Beach, CA, Sept. 23–25 2003, Paper No. AIAA 2003-6329.
- ⁷Wertz, J. R., "High Resolution Structureless Telescope," Tech. Report MC04-1643, NASA/NIAC, April 26 2004.
- ⁸Hyde, R., Dixit, S., Weisberg, A., and Rushford, M., "Eyeglass: A Very Large Aperture Diffractive Space Telescope," *Highly Innovative Space Telescope Concepts*, 2002.
- ⁹Hyde, R., "Eyeglass Large Aperture, Lightweight Space Optics," Tech. Report UCRL-ID-151390, University of California, Lawrence Livermore National Laboratory, Feb. 10 2003.
- ¹⁰King, L. B., Parker, G. G., Deshmukh, S., and Chong, J.-H., "Spacecraft Formation-Flying using Inter-Vehicle Coulomb Forces," Tech. report, NASA/NIAC, January 2002.
- ¹¹Miller, D. W., Sedwick, R. J., Kong, E. M. C., and Schweighart, S., "Electromagnetic Formation Flight for Sparse Aperture Telescopes," *IEEE Aerospace Conference Proceedings – Volume 2*, Big Sky, Montana, March 9–16 2002.
- ¹²Gersh, J., "Architecting the Very-Large-Aperture Flux-Pinned Space Telescope: A Scalable, Modular Optical Array with High Agility and Passively Stable Orbital Dynamics," *AAS/AIAA Astrodynamics Specialist Conference*, Honolulu, Hawaii, Aug. 18–21 2008.
- ¹³Seubert, C. R. and Schaub, H., "Tethered Coulomb Structures: Prospects and Challenges," *AAS F. Landis Markley Astrodynamics Symposium*, Cambridge, MA, June 30 – July 2 2008, Paper AAS 08–269.
- ¹⁴King, L. B., Parker, G. G., Deshmukh, S., and Chong, J.-H., "Study of Inter-spacecraft Coulomb Forces and Implications for Formation Flying," *AIAA Journal of Propulsion and Power*, Vol. 19, No. 3, May–June 2003, pp. 497–505.
- ¹⁵Natarajan, A. and Schaub, H., "Linear Dynamics and Stability Analysis of a Coulomb Tether Formation," *AIAA Journal of Guidance, Control, and Dynamics*, Vol. 29, No. 4, July–Aug. 2006, pp. 831–839.
- ¹⁶Natarajan, A., Schaub, H., and Parker, G. G., "Reconfiguration of a Nadir-Pointing 2-Craft Coulomb Tether," *Journal of British Interplanetary Society*, Vol. 60, No. 6, June 2007, pp. 209–218.
- ¹⁷Tragesser, S. G. and Tuncay, A., "Orbital Design of Earth-Oriented Tethered Satellite Formations," *Journal of the Astronautical Sciences*, Vol. 53, No. 1, Jan. – March 2005, pp. 51–64.
- ¹⁸Menon, C. and Bombardelli, C., "Self-Stabilising Attitude Control for Spinning Tethered Formations," *Acta Astronautica*, Vol. 60, 2007, pp. 828–833.
- ¹⁹Beletsky, V. V. and Levin, E. M., *Dynamics of Space Tether Systems*, Vol. 83, American Astronautical Society, 1993, Advances in the Astronautical Sciences.
- ²⁰Cosmo, M. L. and Lorenzini, E. C., "Tethers in Space Handbook," Tech. report, NASA Marshall Space Flight Center, December 1997.
- ²¹Berryman, J. and Schaub, H., "Static Equilibrium Configurations in GEO Coulomb Spacecraft Formations," *AAS/AIAA Spaceflight Mechanics Meeting*, Copper Mountain, CO, Jan. 23–27 2005, Paper No. AAS 05–104.
- ²²Vasavada, H. and Schaub, H., "Analytic Solutions for Equal Mass Four-Craft Static Coulomb Formation," *Journal of the Astronautical Sciences*, Vol. 56, No. 1, Jan. – March 2008, pp. 7–40.
- ²³Natarajan, A. and Schaub, H., "Hybrid Control of Orbit Normal and Along-Track 2-Craft Coulomb Tethers," *AAS/AIAA Spaceflight Mechanics Meeting*, Sedona, AZ, Jan. 28–Feb. 1 2007, Paper AAS 07–193.
- ²⁴Wang, S. and Schaub, H., "One-Dimensional 3-Craft Coulomb Structure Control," *7th International Conference on Dynamics and Control of Systems and Structures in Space*, Greenwich, London, England, July 16–20 2006, pp. 269–278.
- ²⁵Wang, S. and Schaub, H., "Switched Lyapunov Function Based Coulomb Control of a Triangular 3-Vehicle Cluster," *AAS/AIAA Astrodynamics Specialist Conference*, Pittsburgh, PA, Aug. 9–13 2009.
- ²⁶Gombosi, T. I., *Physics of the Space Environment*, Cambridge University Press, New York, NY, 1998.
- ²⁷Schaub, H., Parker, G. G., and King, L. B., "Challenges and Prospect of Coulomb Formations," *Journal of the Astronautical Sciences*, Vol. 52, No. 1–2, Jan.–June 2004, pp. 169–193.
- ²⁸Valk, S., Lemaître, A., and Deleflie, F., "Semi-analytical theory of mean orbital motion for geosynchronous space debris under gravitational influence," *Advances in Space Research*, Vol. 43, No. 7, 2009, pp. 1070–1082.
- ²⁹Vallado, D. A., *Fundamentals of Astrodynamics and Applications*, Space Technology Library, Springer, 3rd ed., 2007.
- ³⁰Katz, I., Jongeward, G. A., Davis, V. A., Mandell, M. J., Kuharski, R. A., Lilley, J. R., J., Raitt, W. J., Cooke, D. L., Torbert, R. B., Larson, G., and Rau, D., "Structure of the Bipolar Plasma Sheath Generated by SPEAR I," *J. Geophys. Res.*, Vol. 94, No. A2, 1989, pp. 1450–1458, DOI:10.1029/JA094iA02p01450.
- ³¹Olsen, R. C., Van Horn, T., Torbert, R., and Raitt, W. J., "SPEAR-1 Charging Behavior," *ESA Space Environment Analysis Workshop*, Oct. 9–12 1990.
- ³²Schaub, H. and Junkins, J. L., *Analytical Mechanics of Space Systems*, AIAA Education Series, Reston, VA, 2nd ed., October 2009.